NASA Technical Memorandum 107014

Fabry-Perot Interferometer Measurement of Static Temperature and Velocity for ASTOVL Model Tests

Helen E. Kourous and Richard G. Seasholtz
Lewis Research Center
Cleveland, Ohio

Prepared for the
Symposium on Laser Anemometry: Advances and Applications
sponsored by the American Society of Mechanical Engineers
Lake Tahoe, Nevada, June 19–23, 1994

National Aeronautics and
Space Administration

FABRY-PEROT INTERFEROMETER MEASUREMENT OF STATIC TEMPERATURE AND VELOCITY FOR ASTOVL MODEL TESTS

Helen E. Kourous
Richard G. Seasholtz
Optical Measurement Systems
National Aeronautics and Space Administration
Lewis Research Center
Cleveland, Ohio

ABSTRACT

A spectrally resolved Rayleigh/Mie scattering diagnostic was developed to measure temperature and wing-spanwise velocity in the vicinity of an ASTOVL aircraft model in the Lewis 9x15 Low Speed Wind Tunnel. The spectrum of argon-ion laser light scattered by the air molecules and particles in the flow was resolved with a Fabry-Perot interferometer. Temperature was extracted from the spectral width of the Rayleigh scattering component, and spanwise gas velocity from the gross spectral shift. Nozzle temperature approached 800 K, and the velocity component approached 30 m/s. The measurement uncertainty was about 5% for the gas temperature, and about 10 m/s for the velocity. The large difference in the spectral width of the Mie scattering from particles and the Rayleigh scattering from gas molecules allowed the gas temperature to be measured in flow containing both naturally occurring dust and LDV seed (both were present).

INTRODUCTION

Nonintrusive, quantitative techniques for measuring gas parameters are needed for use in aerospace research facilities to provide flowfield characteristics. For example, design of high performance vertical lift aircraft requires knowledge of the temperature and velocity of the lift-generated flowfield in all modes of operation, especially near the engine inlets. When such an aircraft comes into "ground effect" during hover or vertical landing, the lift jets impinge on the ground plane. This may form a fountain of hot gases which act on the underfuselage of the aircraft and recirculate near the aircraft. Depending on conditions, the hot exhaust gases can be ingested by the engine inlets, causing loss of efficiency or catastrophic compressor stall.

An extensive Lewis program was conducted to study the problem of hot gas ingestion for new ASTOVL (advanced short-takeoff vertical landing) aircraft designs. The 12% scale ASTOVL aircraft models were equipped with high temperature and high pressure air supplies to simulate lift nozzles and suction systems to simulate engine inlets. The model under test for the work reported in this paper was a lift plus lift-cruise configuration. It was located in the test section of the Lewis 9x15 Low Speed Wind Tunnel, which is equipped to provide simulated engine and external flow conditions.

The system described in this paper was designed to measure the gas static temperature and the spanwise component of the mean velocity. This velocity measurement was intended to complement measurements made with a separate two-component Laser Doppler Velocimeter (LDV) which measured the other velocity components (vertical and longitudinal). The technique is based on the measurement of the spectrum of laser light scattered by both gas molecules (Rayleigh scattering) and particulates (Mie scattering). A scanning planar mirror Fabry-Perot interferometer was used to measure the spectrum. The width of the Rayleigh scattering component of the spectrum is proportional to the square root of the gas temperature, and the frequency shift of the Rayleigh and Mie spectral peaks from the laser frequency is proportional to one component of the gas and particle velocity. The technique used for these measurements is based on previous work done to measure gas parameters in an hydrogen-oxygen rocket exhaust (Seasholtz et al., 1992; Zupanc and Weiss, 1992).

The optics were placed on a remotely controlled 3D traversing table. This allowed point measurements to be taken at approximately 900 locations in a region under the model encompassing portions of the lift jets, recirculating fountain, engine inlets, and ground-effect flow. An important objective of this work was to demonstrate the feasibility of applying Rayleigh scattering diagnostics in the harsh conditions of a test facility.

The measurements were conducted in two phases. In the first phase, measurements were made primarily to obtain the gas temperature in the vicinity of the model. The front aircraft lift nozzle operated at a pressure ratio of 4.8, with a total temperature of about 800 K (1000 °F). The two rear nozzles operated at a pressure ratio of 2.6. The diameter of each nozzle was about 50 mm. The tunnel headwind velocity was at or below 10 m/s (20 knots). For this phase, no artificial seeding was introduced into the tunnel, and no LDV measurements were made (although significant levels of natural dust were present).

In the second phase, Fabry-Perot and LDV measurements were

taken simultaneously, with the primary goal being the measurement of all three mean velocity components. One micrometer diameter PSL (polystyrene latex) seed was added to both the nozzle and tunnel flow. To prevent degradation of the PSL, the nozzles were operated at less than the design temperature (475 K or 400 °F). So, although temperature data were obtained, they do not represent the design condition temperatures, as was the case for the first phase of measurements.

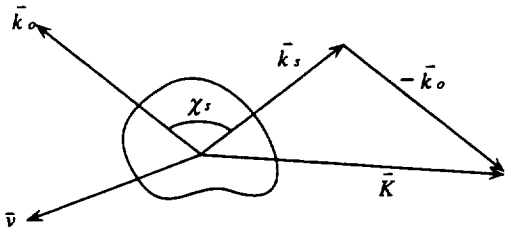

Figure 1. Scattering diagram; $\bar{k}_o$ is the incident wave vector, $\bar{k}_s$ is the scattered wave vector, χ_s is the scattering angle, and $\bar{v}$ is the mean particle velocity. Measured is the projection of $\bar{v}$ along $\bar{K}$.

THEORY

For the Fabry-Perot interferometer based temperature and velocity measurements, a single laser beam is focused at the measurement location (probe volume). Light scattered from gas molecules and particles in the probe volume is collected and its spectrum is measured with the interferometer. The spectrum of the scattered light is broadened by the Doppler shift of the light scattered from the moving gas molecules and particles. For a particle moving with velocity $\bar{v}$, the Doppler shift is given by

$$f_D = \frac{\bar{K} \cdot \bar{v}}{2\pi} \tag{1}$$

where $\bar{K} = \bar{k}_s - \bar{k}_o$ is the wave vector associated with the scattering, $\bar{k}_o$ is the wave vector of the incident laser light, and $\bar{k}_s$ is the wave vector of the scattered light (Figure 1).

For scattering from particles that are all moving with the mean gas velocity, this expression represents the relation between the measured Doppler shift and one component (the component along $\bar{K}$) of the gas velocity. For example, using 476 nm laser light with near-back scatter geometry, the Doppler shift will be 4.2 MHz/m/s.

The light scattered by the gas molecules is likewise Doppler-shifted. For a low density gas with a Maxwellian velocity distribution and where the molecular velocities are uncorrelated, the spectrum is a simple Gaussian. The width of the Gaussian is simply related to the gas temperature by $\Delta f(\text{FWHM}) = 0.265\ Ka$ Hz (Seasholtz et al, 1992), where $a = (2\kappa T/m)^{1/2}$ is the most probable molecular speed (κ is Boltzman's constant and m is the molecular mass). The condition for this low density limit to be valid is that the mean-free-path of the gas molecules be much greater than the interaction wavelength $\Lambda = 2\pi/K$. This condition is usually expressed as the non-dimensional parameter $y = p/(\eta Ka) << 1$, where p is the gas pressure and η is the shear viscosity. However, for the air properties and the optical geometry used in this work, y is on the order of one, and the spectrum cannot be represented by the simple Gaussian. For y values on the order of or larger than one, a more complex spectral model must be used. We used the S6 model developed by Tenti (1974). The FLUID program (Fessler, 1977) was used to calculate the air properties, and the ratio of the shear viscosity to bulk viscosity (required by the S6 model) was assumed to be that of nitrogen at 293 K (given as 1.367 by Boley et al, 1972).

SPECTRAL ANALYSIS USING A FABRY-PEROT INTERFEROMETER

The Fabry-Perot interferometer (Figure 2) is essentially a comb frequency filter whose transmittance depends on the frequency of the incident light, the refractive index μ of the cavity medium, and the mirror separation d. The free spectral range (FSR) is defined as the frequency range between transmittance peaks in the comb filter. The interferometer can be scanned through one FSR by changing the plate spacing by $\lambda/2$ (the phase changes by 2π).

Consider a monochromatic distributed source on the interferometer axis. If the light is allowed to pass through the cavity and is focused with the fringe-forming lens, the image in the focal plane is a series of concentric bright ring fringes, given by the Fabry-Perot transmission function

$$I_t(\psi) = \frac{1}{1 + F\sin^2(\psi/2)} \tag{2}$$

with ψ being the phase delay of the light for one pass through the interferometer given by

$$\psi = \frac{4\pi\mu d f \cos\theta}{c} \tag{3}$$

and $F = (2N/\pi)^2$ where N is the interferometer finesse (Vaughan, 1989). Here f is the optical frequency and c is the velocity of light in free space.

To use the Fabry-Perot interferometer in a scanning mode, a small aperture is located in the focal plane of the fringe-forming lens. Scanning is achieved by varying d at a constant rate through at least one order (FSR) and recording the transmitted light as a function of time. The instrument function is determined by recording the light transmitted through the aperture from a monochromatic source having the same spatial distribution as the scattering source being investigated (Vaughan, 1989).

The measured spectrum S_m consists of the convolution of the actual spectrum (including the Rayleigh/Mie spectrum and the extraneous light at the laser frequency) and the instrument function (Wilksch, 1985). Also included is a broadband term representing background illumination and photomultiplier tube dark current. This can be expressed as

$$S_m(f'_d) = \int \left[G_R S_R(f') + G_P S_P(f')\right] I(f'_d - f')\,df' + G_W I(f'_d) + B \tag{4}$$

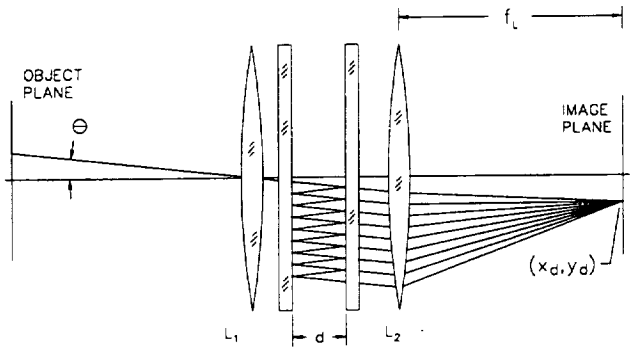

Figure 2. Planar Fabry-Perot interferometer. (x_d, y_d) is the image point, d is the mirror spacing, θ angle of optical ray and optical axis, L_1 is the collimating lens, and L_2 the fringe forming lens.

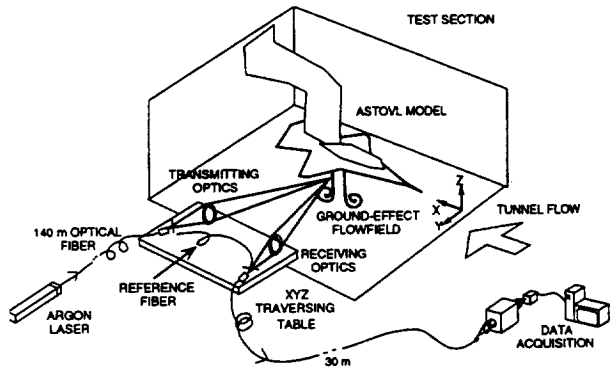

Figure 3. Optical configuration schematic showing wind tunnel test section, scale aircraft model, source laser, optical fibers, reference fiber, traversing table, Fabry-Perot interferometer, and data acquisition system.

where $f' = f - f_o$ is the relative frequency shift from the laser frequency f_o, and $f'_d = f_o(1 - d/d_o)$ is a scanning parameter related to the physical cavity spacing d. Here G_R and $S_R(f')$ are the total scattered power and spectrum of the Rayleigh scattered light; G_P and $S_P(f')$ are the total scattered power and spectrum of the Mie scattered light (from particles); G_w is the power of elastically scattered light at the laser frequency from surfaces and walls; B is the broadband background, which includes photomultiplier dark current; and $I(f'_d)$ is the Fabry-Perot instrument function.

FACILITY DESCRIPTION

The system was deployed in the Lewis Research Center 9x15 Low Speed Wind Tunnel. The test section was 2.7 x 4.6 x 6.1 m (9 x 15 x 20 ft.) and had lateral flow dumps (gaps in the flush acoustic boxes). To achieve optical access, one side of the tunnel test section had several rows of the acoustic boxes removed. The optics for both the LDV and the Fabry-Perot based system were arranged on a 3D traversing table. The measurement region spanned a volume under the model 17 cm spanwise (along the wingspan direction), 150 cm longitudinally, and 15 cm vertically (starting about 2 cm below the front nozzle exit plane). The model was suspended in the test section by an integrated support system which allowed for pitch, yaw, roll, and altitude adjustment, as well as high-temperature simulated lift nozzles and engine inlet draw. For the work reported here the model was configured at zero pitch yaw and roll, and was positioned 66 cm above the ground plane (measured to the nose). See Figure 3.

The model was equipped with three simulated-lift nozzles, indicated in Figure 4. Main inlets were positioned near the fuselage and wing-body joint, while auxiliary inlets (to open during ground effect) were positioned with a horizontal inlet plane near the wing leading edge. The model landing gear was removed for the laser-based tests. The tunnel and nozzle flow consisted of ambient air (nozzle flow heated by gas heat exchanger).

OPTICAL CONFIGURATION

The components of the optical delivery and receiving system are shown in Figure 3. The laser was in a remote location vibrationally isolated from the wind tunnel. The optical power was delivered via silica/silica multimode fiber, core diameter 200 μm, numerical aperture 0.22, to the test section 140 m away. The beam was expanded from the polished end of the delivery fiber into a 150 mm diameter lens pair. The focal lengths of the lenses were 450 and 2200 mm, giving a magnification factor of about five. Thus, the probe volume diameter (at working distance 2200 mm) was 1 mm and the length was about 4 mm. The laser beam was focused at a point in the region under the aircraft and then absorbed by a blackened region beyond the section wall to minimize the amount of non-Rayleigh-scattered laser light entering the receiving optics.

Scattered light was collected in near-backscatter mode at a 149.9° scattering angle. The receiving optics, a lens pair identical to the transmitting optics, imaged the probe volume onto a 200 μm-core collection optical fiber.

In addition, translucent diffusers were mounted on pneumatic actuators to intercept the expanding power beam and were used periodically to inject a small amount of laser light directly into the signal-receiving fiber via the reference fiber (reference signal is discussed in the data acquisition section). The optics, as shown in Figure 3, were mounted on a 3D traversing table. The scattered light was then delivered to the auxiliary control room (some 30 m away) for conversion and data processing in a vibration-isolated environment where the Fabry-Perot interferometer, collimating lenses, pinhole, photomultiplier tube, and data acquisition PC were located.

For the temperature measurements (first phase of the test), the argon-ion laser was operated at 488 nm at 2.3 W (higher power could be achieved but resulted in laser lineshape degradation), with power at the probe volume of 1 W. For the velocity measurements (phase two) laser output power was 1.8 W, and 0.7 W was delivered to the probe volume. Here the laser was operated in single-line mode at 476.5 nm. The single axial mode operation needed for spectral measurements was achieved via a temperature-tuned intracavity etalon. The LDV system used for the other two velocity component measurements utilized the 488 nm and 514.5 nm lines of a separate argon-ion laser.

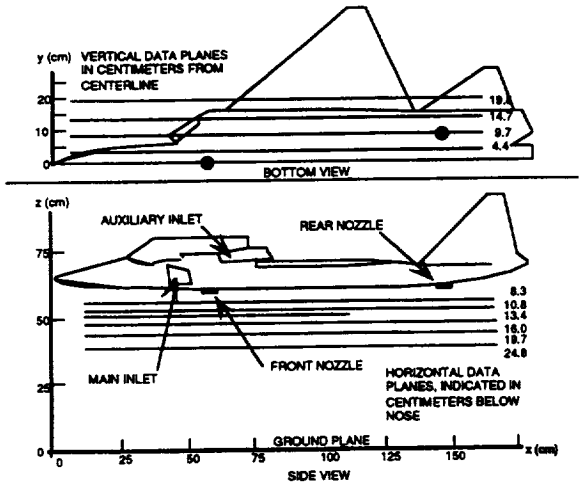

Figure 4. Measurement locations. Note the lift nozzles at x = 57 cm and at x = 142 cm. Point samples were taken in the x direction along the projected planes shown; typically denser in nozzle flow region and more sparse in the outermost planes.

In the auxiliary control room, the Fabry-Perot interferometer was set up in a thermal enclosure on a vibration isolation table, along with collimating and fringe-forming lenses (160 mm focal length). The signal beam expanded from the 0.22 NA polished fiber end into the collimating lens and was passed through the Fabry-Perot interferometer (15.1 mm plate spacing, 50 mm aperture, and 90% reflectance) and focusing lens, and then through a 0.25 mm diameter pinhole to the photomultiplier tube. In addition, for the velocity measurement phase, a 476.5 nm wavelength interference filter was used to exclude the LDV wavelengths.

DATA ACQUISITION

The Fabry-Perot mirror spacing was mechanically scanned through a ramp waveform via piezoelectric actuators and a high voltage ramp generator. The scan rate was one per second. The ramp was chosen such that the interferometer scanned through two free spectral ranges (or bandpass orders), amounting to about 20 GHz. The photomultiplier tube was used in photon-counting mode, with counts accumulating in fixed time intervals during the scan. The counts from each interval were transferred from the photon counter to the computer via a parallel interface and stored in 100-bin histograms. Each scan was stored as a separate histogram.

Groups of 20 scans were taken, with scans 1-3 and 18-20 being reference scans of the unshifted laser light, and scans 5-16 being data scans of light scattered from the probe volume (scans 4 and 17 were not used because the system was automatically switched between the reference and data signals at these times). Typically three sets of 20 scans were taken at each spatial location of the traversing table, for a total acquisition time per location of about 70 seconds. Figure 5 shows sample reference and data spectra. The reference fiber mentioned earlier serves the purpose of injecting unshifted laser light directly into the data acquisition system for the first three and last three interferometer scans of the

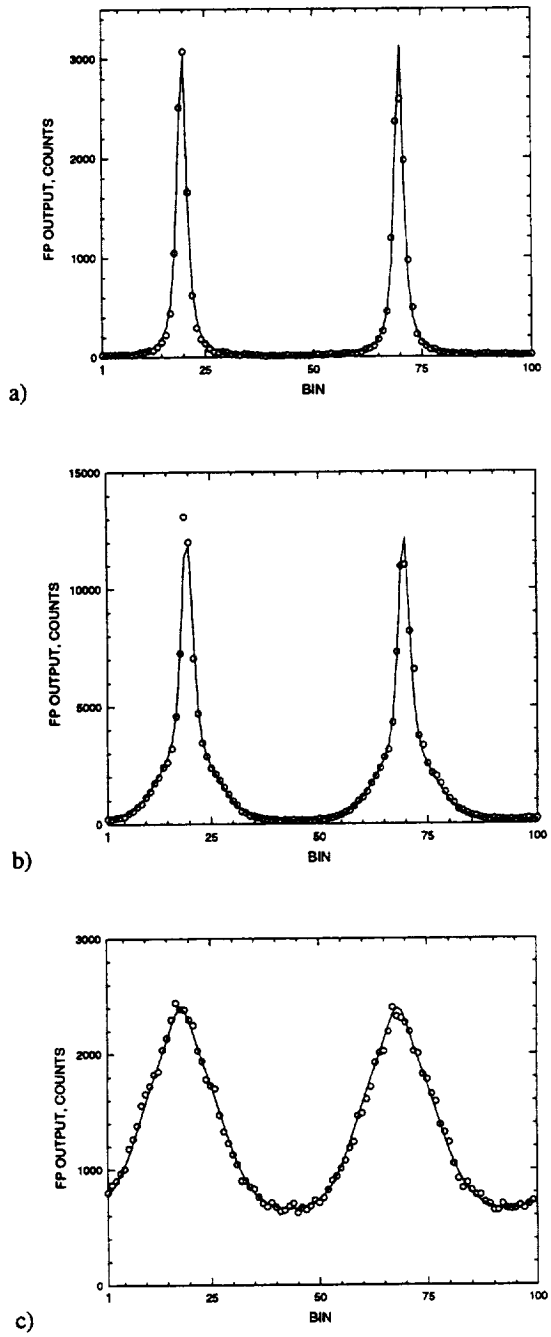

Figure 5. Spectra acquired by the Fabry-Perot interferometer: a) measured instrument function; (b) a Mie-dominated seeded-flow spectrum; and (c) a high temperature Rayleigh-dominated spectrum in unseeded flow.

20-scan data point.

DATA PROCESSING

The following steps were used to process the spectral data. Obtained were estimates of the gas temperature and velocity

component along the viewing direction.

1) The 20 scans in each group were combined to form three spectra: a reference spectrum at the beginning of the group (from scans 1-3), a reference spectrum at the end of the group (scans 18-20), and the data spectrum from scans 5-16.

2) A 4-parameter least squares fitting procedure (Beck and Arnold, 1977) was applied to each of the two reference spectra to obtain the peak position of the unshifted laser light, the free spectral range, and the finesse of the interferometer. The determination of these parameters at the beginning and end of the group allowed detection of changes in the unshifted laser frequency and FSR that might have occurred during the data acquisition.

Change greater than a predetermined amount was cause for rejection of the data group. The averages of these initial and final values of peak position, finesse, and FSR were calculated for use in the next step. These parameters were also used to calculate the instrument function of the interferometer.

3) A 6-parameter least squares fit was then applied to the data spectrum. The model of the measured spectrum used (equation 4) was the convolution of a model of the spectrum of the collected light and the instrument function of the interferometer (obtained in step 2). Poisson statistics were used for the noise model. The spectrum model included: the Rayleigh scattered light, where the spectral shape was obtained using the Tenti S6 model (Tenti, 1974); the light scattered from particles; and a constant broadband signal.

The mean velocity of the gas and particles was assumed to be equal, and the extraneous light at the laser frequency, G_w was assumed to be negligible. Finally, a broadening parameter was included to account for turbulence and for jitter in the interferometer that might have occurred during the data acquisition. In the absence of jitter, this parameter could be used to determine turbulence intensity.

This procedure gives estimates of the parameters of interest – the gas temperature and the velocity component along $\vec{K}$. Estimates of the uncertainty in these parameters caused by the photon-statistical noise are also obtained. Figure 5 shows the fit for two cases, as well as the instrument function (5a). Figure 5b was obtained at a location with a relatively large particle number density, and Figure 5c was obtained while the probe volume was in the nozzle flow, where the spectrum is primarily of Rayleigh scattered light.

MEASUREMENT UNCERTAINTY

The photon statistical shot noise mentioned in the data processing section results in a fundamental lower bound on the measurement uncertainty. These uncertainties were obtained from the least squares parameter estimation procedure. In general, other factors will increase the measurement uncertainty. One important factor is the physical stability of the Fabry-Perot interferometer during data acquisition. Thermal changes, vibration, and lack of exact repeatability in the scanning can cause variation in the unshifted laser frequency location in the recorded spectrum and in the finesse. This results in an uncertainty in the velocity measurement, which is based on the frequency shift of the scattered light from the laser frequency. The error in velocity caused by an error in the unshifted laser frequency f_o is seen from equation (1) to be

$$\delta V = \frac{2\pi}{K}\delta f_o \tag{5}$$

Sets of reference spectra were taken at various occasions during the test. Analysis of some of these spectra showed a typical rms variation in f_o of about 20 to 40 MHz, which corresponds to a velocity uncertainty of 5 to 10 m/s. Because the δf_o-induced uncertainty was significantly greater than the shot-noise-induced uncertainty (2-3 meters per second) it alone was used as the velocity uncertainty.

Another potential error source is the random rate of arrival of the particles passing through the probe volume. Errors occur when the number of particles in the probe volume is on the order of one, which can cause a false indication of the particle signal peak location in the spectrum. For this test, however, the number of particles in the probe volume at any given time was generally large (particularly when the flow was seeded), and it is believed that this error is not significant. Only in the nozzle flow was the particle number density low and, again, no significant error should occur because the velocity is obtained from the relatively large Rayleigh peak which exists in this region.

We believe that the relatively large estimated uncertainty in the temperature measurements due to shot noise (typically about 5%) was larger than other potential error sources. The shift in f_o which was an important factor in the velocity measurement uncertainty, should not affect the temperature measurement because only the spectral width (not the spectral position) enters into the temperature calculation. In summary, the shot-noise uncertainty calculated from the parameter estimation was used as the temperature measurement uncertainty (about 5%), while the δf_o-induced uncertainty (about 10 m/s) was used as the velocity uncertainty.

RESULTS

Some preliminary data are presented to illustrate the technique. The data shown represent a fraction of the total data sets taken, which number about 2500 spectra.

Figure 6 shows Rayleigh temperature data for several longitudinal (along the long axis of the aircraft) scans of the traversing table, and Figure 7 shows velocity data. The velocity measurements showed that the spanwise component was generally quite small. This was expected because the flow was primarily along the tunnel axis in the regions where measurements were made, whereas the measurement direction was spanwise. Limitations in optical access prevented measurements from being taken near the ground plane where the spanwise component was assumed to have been large. Also, no measurements were taken at locations where the laser beam terminated on the model body.

The first phase measurements show the elevated temperatures in the nozzle flow. Note that the front nozzle data indicate higher temperatures than the rear nozzle data for the y plane of 10 cm. In addition, there is a general increase in temperature toward the rear of the model (increasing x).

Assuming fully expanded isentropic flow, the exit-plane temperature for the front nozzle (pressure ratio 4.8) can be calculated to be 520 K. This is in good agreement with the temperature peaks shown in Figure 6 which correspond to spatial locations directly under the front nozzle.

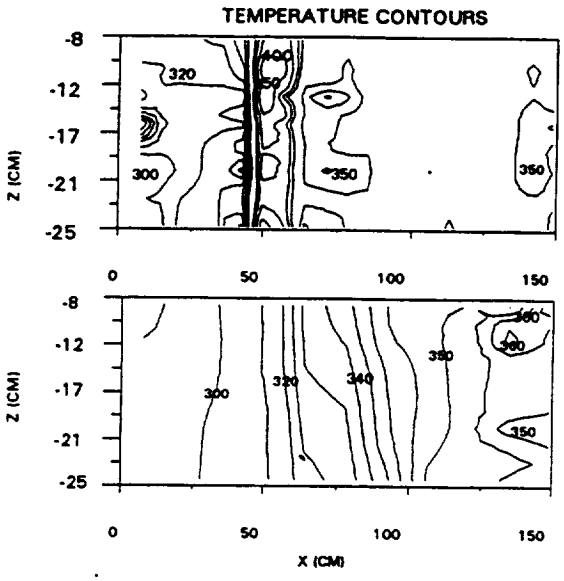

Figure 6. Measured temperature for a planar region under the model along the longitudinal centerline (y=0); nozzle flow is vertical at x = 57 cm. The second plot shows a plane (y = 9.7 cm) cutting through the centerline of the rear nozzle; the nozzle is at x = 142 cm.

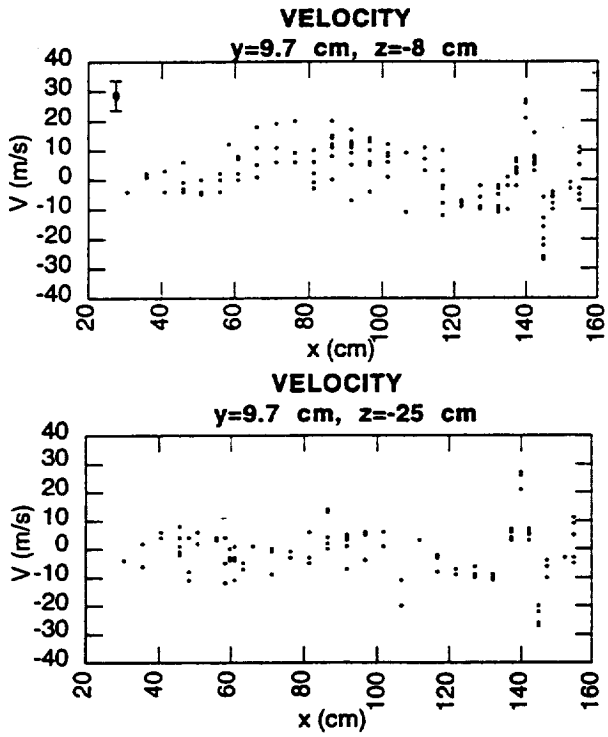

Figure 7. Velocity data for y=9.7 cm out from centerline, z = -8 and -25 cm (measured vertically from model nose).

CONCLUDING REMARKS

The system described in this paper demonstrated the viability of using Rayleigh scattering to measure gas temperature in flows that contain significant concentrations of micrometer size particles. This was due to the large difference in spectral width of the Mie and Rayleigh scattering peaks which allowed temperature information to be extracted from the combined spectrum. The uncertainty in the gas temperatures was about 5%.

The system also was able to measure the line-of-sight mean velocity component with about 10 m/s uncertainty. Note that the uncertainty is independent of the velocity, and thus would give much smaller relative errors for higher speed flows. In addition, better thermal and vibration control of the Fabry-Perot interferometer should reduce this error to the shot noise limit of 2-3 m/s. It is worth mentioning that we found fiber optic transmission of the laser light to be a very effective method of isolating both the source laser and the interferometer from the noisy wind tunnel environment.

ACKNOWLEDGMENTS

We would like to thank Barbara Esker, Al Johns, and George Neiner for the opportunity to take data in the wind tunnel facility. We would like to acknowledge all those whose assistance was invaluable: Andrew Kremer, Martin Krupar, Gary Podboy, Vic Canacci, Wendy Grosser, and the entire 9 x 15 crew. We also wish to thank Prof. G. Tenti for kindly providing us with the computer program for calculating the S6 model spectrum.

REFERENCES

Beck, J.V., and Arnold, K.J., 1977, *Parameter Estimation in Engineering and Science*, John Wiley & Sons, New York, pp. 259-269.

Boley, C.D., Desai, R.C., and Tenti, G., 1972, "Kinetic models and Brillouin Scattering in a Molecular Gas", *Can. J. Phys.*, vol. 50, pp. 2158-2173.

Fessler, T.E., 1977, "FLUID: A Numerical Interpolation Procedure for Obtaining Thermodynamic and Transport Properties of Fluids," NASA TM X-3572.

Seasholtz, R.G., Zupanc, F.J., Schneider, S.J., 1992, "Spectrally Resolved Rayleigh Scattering Diagnostic for Hydrogen-Oxygen Rocket Plume Studies," *AIAA Journal of Propulsion and Power*, Vol. 8, No. 5, Sept.- Oct. 1992, pp. 935-942.

Tenti, G., Boley, C.C., and Desia, R. C, 1974, "On the Kinetic Model Description of Rayleigh-Brillouin Scattering from Molecular Gases," *Can. J. Phys*, 52, pp. 285-290.

Vaughan, J.M., 1989, *The Fabry-Perot Interferometer: History, Theory, Practice, and Applications*, Adam Hilger, Bristol, 1989, Chapter 3.

Wilksch, P. A., 1985, "Instrument function of the Fabry-Perot spectrometer", *App. Op.*, V24, No. 10, 15 May 1985, pp. 1502-1511.

Zupanc, F.J. and Weiss, J.M., 1993, "Rocket Plume Flowfield Characterization Using Laser Rayleigh Scattering", *28th Joint Propulsion Conference*, July 6-8, 1992, Nashville, TN, AIAA paper 92-3351.

REPORT DOCUMENTATION PAGE

Form Approved
OMB No. 0704-0188

1. AGENCY USE ONLY (*Leave blank*)	2. REPORT DATE	3. REPORT TYPE AND DATES COVERED
	July 1995	Technical Memorandum

4. TITLE AND SUBTITLE

Fabry-Perot Interferometer Measurement of Static Temperature and Velocity for ASTOVL Model Tests

5. FUNDING NUMBERS

WU-505-62-50

6. AUTHOR(S)

Helen E. Kourous and Richard G. Seasholtz

7. PERFORMING ORGANIZATION NAME(S) AND ADDRESS(ES)

National Aeronautics and Space Administration
Lewis Research Center
Cleveland, Ohio 44135-3191

8. PERFORMING ORGANIZATION REPORT NUMBER

E-9799

9. SPONSORING/MONITORING AGENCY NAME(S) AND ADDRESS(ES)

National Aeronautics and Space Administration
Washington, D.C. 20546-0001

10. SPONSORING/MONITORING AGENCY REPORT NUMBER

NASA TM-107014

11. SUPPLEMENTARY NOTES

Prepared for the Symposium on Laser Anemometry: Advances and Applications sponsored by the American Society of Mechanical Engineers, Lake Tahoe, Nevada, June 19–23, 1994. Responsible person, Richard G. Seasholtz, organization code 2520, (216) 433–3754.

12a. DISTRIBUTION/AVAILABILITY STATEMENT

Unclassified - Unlimited
Subject Category 35

This publication is available from the NASA Center for Aerospace Information, (301) 621-0390.

12b. DISTRIBUTION CODE

13. ABSTRACT (*Maximum 200 words*)

A spectrally resolved Rayleigh/Mie scattering diagnostic was developed to measure temperature and wing-spanwise velocity in the vicinity of an ASTOVL aircraft model in the Lewis 9×15 Low Speed Wind Tunnel. The spectrum of argon-ion laser light scattered by the air molecules and particles in the flow was resolved with a Fabry-Perot interferometer. Temperature was extracted from the spectral width of the Rayleigh scattering component, and spanwise gas velocity from the gross spectral shift. Nozzle temperature approached 800 K, and the velocity component approached 30 m/s. The measurement uncertainty was about 5% for the gas temperature, and about 10 m/s for the velocity. The large difference in the spectral width of the Mie scattering from particles and the Rayleigh scattering from gas molecules allowed the gas temperature to be measured in flow containing both naturally occurring dust and LDV seed (both were present).

14. SUBJECT TERMS

Fabry-Perot interferometers; Laser anemometers; Short takeoff aircraft; Wind tunnel tests

15. NUMBER OF PAGES

8

16. PRICE CODE

A02

17. SECURITY CLASSIFICATION OF REPORT	18. SECURITY CLASSIFICATION OF THIS PAGE	19. SECURITY CLASSIFICATION OF ABSTRACT	20. LIMITATION OF ABSTRACT
Unclassified	Unclassified	Unclassified	